5-6-2024

Introduction to 2D and 3D Nanomembrane Devices: Fabrication and Characterization

Noah Zheng
Washington University in St. Louis

Washington University in St. Louis

James McKelvey School of Engineering

Spring 2024 MEMS 400 Independent Study

Introduction to 2D and 3D Nanomembrane Devices: Fabrication and Characterization

Noah Zheng, B.S. Mechanical Engineering

Principal Investigator: Dr. Sang-Hoon Bae; Advisor: Dr. Sangmoon Han

Department of Mechanical Engineering and Materials Science

ABSTRACT

The goal of this independent study was to gain familiarity with research methods and fundamental concepts in 2D/3D materials research. To that end, two projects were completed – 1) the design, fabrication, and characterization of an in-vivo flexible piezoelectric antenna, and 2) the fabrication and characterization of a GaN-based, interdigitated (IDT), surface acoustic wave (SAW) strain sensor. The function of the in-vivo antenna was successfully demonstrated. The SAW strain sensor's basic functionality was also demonstrated, but performance was modest. Alongside in-lab work, the operating principles behind the devices and the state of 2D/3D nanomaterials research were studied at an introductory level through literature review. The following report documents important theoretical concepts learned, in-lab methods, and the testing results for the two devices.

INTRODUCTION

2D and 3D Freestanding Nanomembranes

2D and 3D are classifications for crystalline materials. Most crystals are 3D – their covalent bonds extend in all three dimensions. These crystals can grow indefinitely in any direction. However, some materials' crystal structures are confined to a planar geometry, which makes them "2D". Of course, these materials still have thickness, but their structures do not allow covalent bonds to extend out of the plane. The bulk forms of 2D materials, then, consist of many stacked layers of planar crystals connected by van der Waals forces. Since no covalent bonds link the layers, they can be easily separated with several techniques, such as mechanical- and liquid exfoliation. When 2D crystals are isolated as a single atomically thin layer, its properties change in useful ways compared to the bulk form. This form factor has also been extended to 3D materials: although they don't naturally separate into layers per se, 3D materials as nanomembranes benefit from being transparent and flexible [1].

2D Materials	3D Materials
• Naturally layered • Covalent bonds only occur in a plane • Monolayer properties are significantly different compared to bulk • Atomically smooth surface	• Not naturally layered • Covalent bonds connect all atoms in the lattice • Thin membranes retain bulk properties • More difficult to create nanomembranes • Dangling covalent bonds occur at layer surfaces

Figure 1 – Table comparing aspects of 2D and 3D materials. A similar table from which this information was derived can be found in Meng et al. [1]

Conventional materials and architectures used in electronics are approaching limits in performance, power consumption, and miniaturization. Effects such as current leakage and high resistance at electrodes hinder device capabilities. Research has been looking into using 2D/3D nanomembrane heterostructures – devices that combine multiple layers of atomically thin materials – to replace current technology using Si-based semiconductors. Benefits range from reducing contact resistance to unlocking quantum properties only useful at atomic thicknesses, such as spin-polarized current [2]. And because these nanomembranes are so thin, they

have the natural advantage of being small, flexible, and transparent, making them suitable for bio-compatible applications.

More specifically, vertically stacked heterostructures coupled only by van der Waals forces have been of great interest. Without covalent/dangling bond clamping effects on the functional 2D or 3D layer, the desirable properties of such materials are amplified [3]. Van der Waals direct mechanical stacking also allows many more combinations of materials compared to traditional epitaxy – while adjacent materials' crystal structures have to be closely similar for epitaxy [3], this can be disregarded with van der Waals heterostructures [1]. By growing each layer separately (and freestanding by using remote epitaxy) and putting them together later, defects with heteroepitaxy such as amorphous growth and polycrystallinity can be avoided, as long as the transfer techniques are successful. Layers can also be stacked with various rotational offsets, resulting in moiré patterns that behave specially [1]. Theoretically, any number of layers of various 2D and 3D materials can be stacked together to form devices for a variety of purposes, from photovoltaics to neuromorphic AI processors. There is, after all, a large library of 2D and 3D materials to choose from, with properties running the gamut.

One of the biggest setbacks to wide implementation of 2D and 3D nanomembranes is commercial viability. The fabrication methods for these materials are difficult to scale up – remote epitaxy on certain growth substrates, for example. Techniques for making nanomembranes out of 3D materials also need to be refined [1]. That aside, these materials have great potential to supersede today's electronics in unexpected ways.

IN-VIVO FLEXIBLE ANTENNA

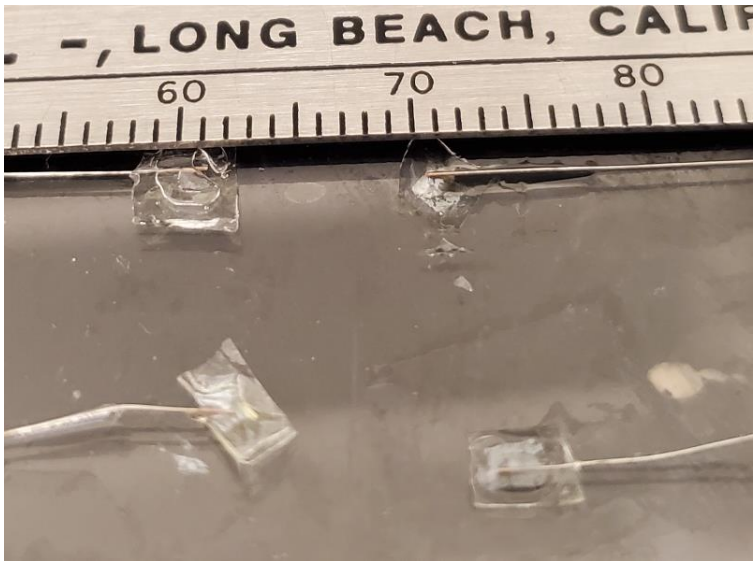

Figure 2 - picture of four prepared antennae. Overall device thickness is ~ 80-200μm. Device width is 3-5mm per side.

Fabrication

Overview of Device Structure: The goal of the device is to function as an antenna while implanted in an animal. Thus, the device needs to be small, flexible, and biocompatible. The device consists of a thin substrate layer of PDMS (polydimethylsiloxane), on top of which the following layers are transferred: 2 monolayers of MoS_2 (0.7 nm thick) and 1 layer TiO_2 (30 nm thick). Following this is a thin wire that extends out of the device. Finally, the setup is enclosed by four "walls" and a "ceiling" of PDMS to protect the functional layers in-vivo. Four final devices were produced.

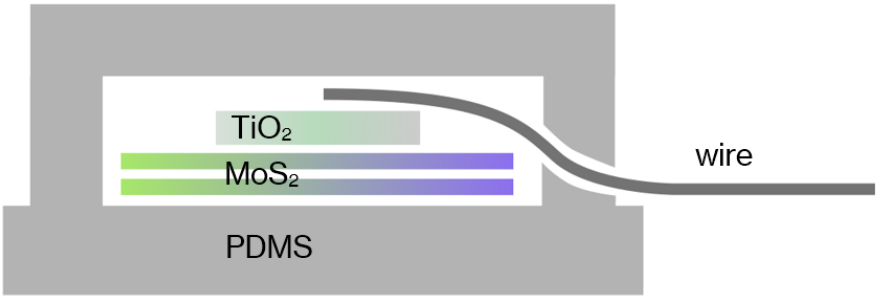

Figure 3 – Left: Diagram of antenna components. Not to scale due to vastly different layer thicknesses.

What is a Piezoelectric Antenna, and why is it needed? The most common type of antenna is electric, which operates based on oscillating currents within the conducting material of the device. For acceptable levels of efficiency, the size of an electrical antenna needs to be at least 1/10 of the operating wavelength. Smaller sizes are drastically less efficient, which makes it quite difficult to transmit low-megahertz frequencies (whose wavelengths range from tens to thousands of meters) with any device small enough to be implantable [4]. Because the operating frequency of our antenna happens to be in this range, another method of transmission is needed. Note that it is also undesirable to increase the operating frequency into the GHz range, as GHz frequencies cause molecular rotations and vibrations which heat up live tissues [5]. In addition, higher frequencies result in greater propagation loss, which diminishes range [5]. Thus, GHz frequencies are a no-go for an in-vivo antenna.

Piezoelectric antennae have been shown to have good efficiencies even at small sizes. In fact, they can be up to 10^5 times smaller than an electrical antenna for a given frequency [4]. For two antennae of the same size, Hassanien et al. [4] demonstrated a piezoelectric antenna that was 6000 times more efficient than its electrical counterpart. This efficiency increase enables small implantable antenna operating in the low MHz range to be feasible.

The enormous efficiency increase is thanks to the fact that acoustic waves propagate 10^5 times slower than EM waves [4]. In a piezoelectric antenna, the voltage input signal does not directly cause charge acceleration. Instead, the oscillating voltage signal gives rise to mechanical oscillations in the antenna's material thanks to the piezoelectric effect. As the piezoelectric element changes shape, it becomes polarized in one direction or the other, and the net effect is that of an oscillating dipole moment at the same frequency of the mechanical vibration. This oscillating dipole moment in turn generates the propagating EM wave. High efficiency is achieved when the acoustic resonance of the antenna is set to match the input signal.

Justification of Materials: PDMS is an easy-to-fabricate polymer that is highly flexible, transparent, and can be made into very thin membranes. It is also relatively biocompatible, allowing the antenna to be implanted into an animal. The functional layer, TiO_2, was chosen for its high piezoelectric constant d_{33}, which better couples the input signal to acoustic energy and back into emitted radiation. The layers of 2D MoS_2 between the PDMS and TiO_2 serve as a barrier preventing dangling bonds on each side from interacting with each other. The TiO_2 is thus made more freestanding, and its piezoelectric properties are less hindered by mechanical binding to other

layers: The only interaction desired between the TiO_2 and surrounding layers are weak van der Waals forces. When compared to a similar device in which the TiO_2 is covalently bonded to a rigid substrate, the freestanding device's piezoelectric and magnetostrictive responses are approximately 10 times larger [3]. Two layers of MoS_2 were found to be more effective than one layer also due to imperfections in the fabrication of the device – when the 2D material was transferred onto the PDMS substrate, there were often small imperfections where the MoS_2 failed to attach to the PDMS, and the second layer helped to cover areas left bare by the first.

PDMS Substrate Preparation: 10 parts base (by mass) and 1 part agent of the SYLGARD™ 184 Silicone Elastomer Kit from Dow were weighed and combined in a petri dish. To remove bubbles formed during mixing, the mixture was pulled under vacuum for 3 cycles of ~5 minutes each. This viscous, highly transparent mixture gradually cures at room temperature but stays liquid for a few days, allowing for adjustment and reuse. Curing can be accelerated to finish in about 5 minutes by heating at ~120° C.

To prepare films for the substrate and ceiling, a glass slide was spin-coated with the PDMS at 800rpm for 60 seconds, then cured on a hot plate. The individual substrates were then cut using a razor blade and peeled off the glass slide using tweezers.

MoS_2 (2D Material) Transfer: the source of monolayer MoS_2 was a wafer of Si-SiO_2 with a layer of MoS_2 and a handling layer of PMMA (polymethyl methacrylate) on top. Approximately 5mm x 5mm squares of the wafer were cut by successively scoring the top surface with a diamond cutter and stressing the wafer until it snaps at the score lines (the exact size is not crucial – the MoS_2 must only be large enough to provide a place for the TiO_2 to sit. The edges of these square samples were scraped with tweezers to loosen the edges for lift-off. The samples were then slowly dipped into a dish of deionized (DI) water. As the sample is submerged, the MoS_2-PMMA separates from the Si-SiO_2 below and floats on the surface of the water. At this point, the samples were ready to be transferred to the target PDMS substrate.

For transfer, one target PDMS substrate was laid flat on a glass slide and submerged into the dish containing the MoS_2. Using tweezers, a square of MoS_2 was gently moved over the target substrate. Holding the MoS_2 in place, the glass slide was slowly lifted out of the water so that the MoS_2 was scooped up from below. The procedure was repeated for the remaining samples. All samples were then left to dry – as the water between the PDMS and MoS_2 evaporates, the two layers come into close contact, and the desired interlayer van der Waals interactions

form, securing the two layers together. The samples were then submerged in acetone and heated at 40° C for 30 minutes until the PMMA handling layer was etched away.

The process was then repeated for the second layer of MoS_2. Care was taken to place the second layer of MoS_2 as directly as possible on top of the first layer.

Figure 4 – Photos at select steps of the MoS_2 transfer process. From left to right: 1) two squares cut from the larger wafer, with the green one yet to be lifted off; 2) MoS_2-PMMA membrane floating in water; 3) two samples recently transferred with water still present; 4) two samples with two layers of MoS_2 transferred and dried.

Note: due to the transparent nature of both the substrate and the nanomembranes, it can be very difficult to determine which side is “up” in case a sample gets flipped over. An observation with the MoS_2 is that the top side has a slight blue-violet sheen when viewed from certain angles. Viewed from the other side, the patch of MoS_2 remains as usual – a transparent yellow-green tint.

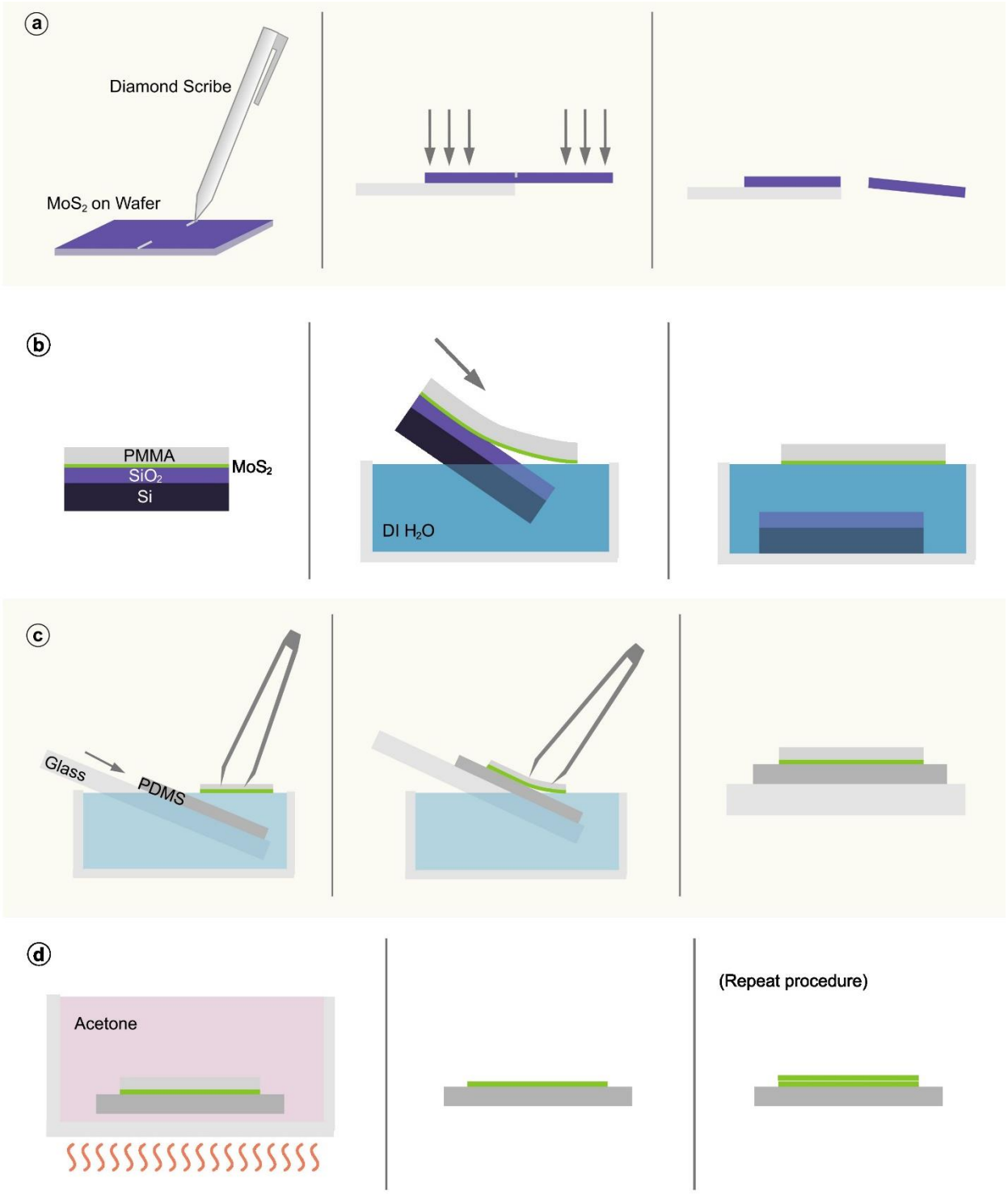

Figure 5 – Illustration of the MoS_2 transfer process. a) Procedure for cutting wafers into desired size. b) Lifting off MoS_2 from source substrate. c) Transferring to PDMS. d) Etching PMMA and repeating procedure for second layer of MoS_2.

TiO_2 (3D Material) Transfer: The TiO_2 layer was sourced from a wafer of Si-SiO_2, upon which Ni and TiO_2 were successively deposited, and thereupon a handling layer of PPC (polypropylene carbonate). Based on the desired resonant frequency of the antenna, it was determined that the 3D layer should be a square of 2mm x 2mm. After cutting the square samples from the wafer, the samples were submerged in a dish of DI water. The TiO_2 film does not lift off as easily as the MoS_2, so tweezers were needed to manually peel it off. The goal is to have the Ni-TiO_2-PPC layers detach cleanly from the Si-SiO_2 wafer and float on the surface of the water.

After liftoff, the Ni underneath the TiO_2 needs to be etched away. This was done by floating the samples in a dish of ferric chloride copper etchant solution (supplier: MG Chemicals). To transport the samples between petri dishes, a scrap piece of a silicon wafer held by plastic tweezers was used to scoop the samples out of one liquid and float them onto the surface of another liquid. After approximately one minute, the samples turned transparent, indicating that the Ni had fully reacted. The samples were then rinsed clear of the etchant by three successive "baths" in dishes of fresh DI water (the samples were floated on the water's surface). After rinsing, the samples were transferred to the target substrate using the same procedure as for the MoS_2, taking care to place the TiO_2 wholly on the 2D material below. The samples were then dried, and the PPC handling layer was etched off in anisole (similar technique to the PMMA-acetone etching).

Wiring and sealing: a ~5 cm length of thin wire was laid on top of the TiO_2 layer. Using the remaining uncured PDMS mixture from earlier in the process and a pair of tweezers, a liquid PDMS barrier was dabbed in an outline around the square of TiO_2. The barrier was then cured by placing the samples on a hot plate at 120° C for a few minutes. Meanwhile, squares were cut from the same PDMS spin-coated glass slide used for the substrate – these would serve as the "ceiling" of the device. After curing, a small additional amount of uncured PDMS was dabbed on top of the barrier as an adhesive for the ceiling, and the cut squares of PDMS were placed on top. After undergoing one final curing, the devices were sealed.

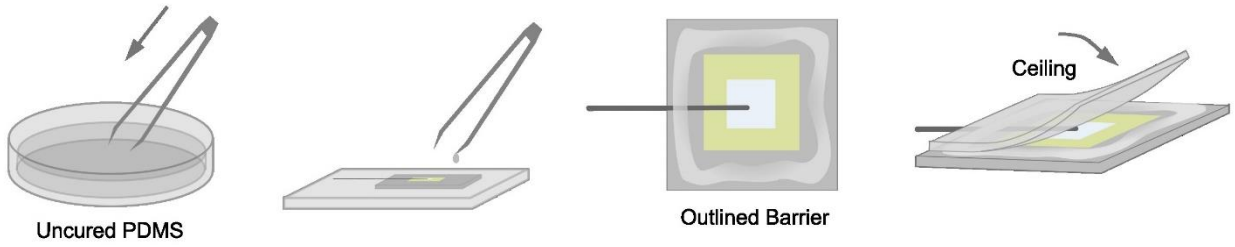

Figure 6 – Device sealing process, illustrated.

Analysis

Resonant Frequency: A NanoVNA (Vector Network Analyzer) was used to evaluate the antenna's performance. The NanoVNA supplied an input signal and measured the reflected signal to determine the extent of impedance mismatch and the antenna's optimal operating frequencies. The input signal was swept from 50 kHz to 10 MHz.

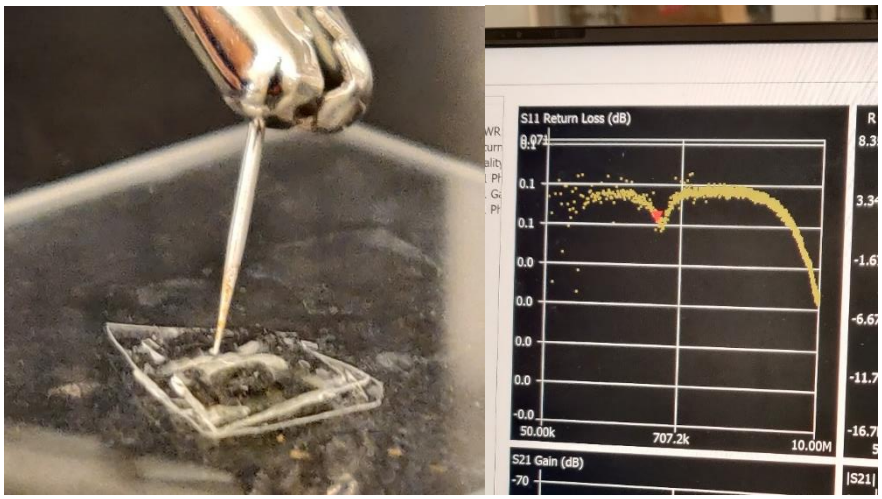

Figure 7 – Left: Close-up picture of testing apparatus from an early version of the antenna. The first port of the NanoVNA was connected to a coaxial cable which in turn connected to the alligator clip/needle probe as shown. The probe was then contacted gently with the top surface of the device. Right: Graph of S11 return loss vs. input signal frequency. There appears to be a resonance somewhere slightly less than 700 kHz.

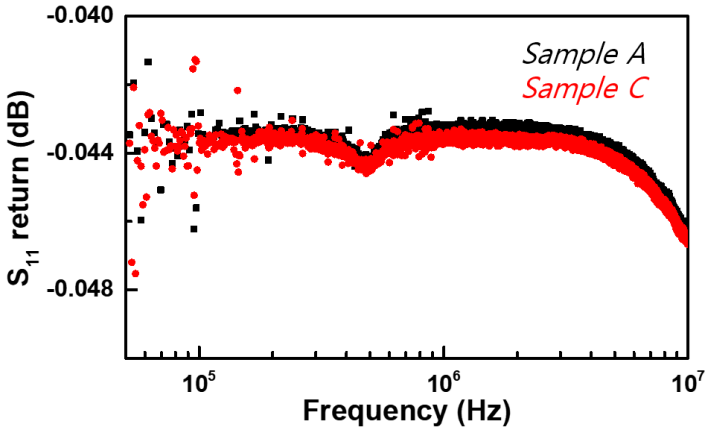

Figure 8 – A very modest trough in the S_{11} return loss graph for two of the antennae is observed at an input frequency of around 500 kHz. Sample A and Sample C were among the final four devices produced – not all devices were successful.

Applications and Further Study: The in-vivo antenna is a versatile device that can be paired with flexible biocompatible sensors to create health monitoring systems. As the device has been successfully miniaturized to function in mice, it is likely already small enough for many applications in larger animals. However, the fabrication process is by no means perfected. Further study should examine ways to increase the precision of the membrane sizing (currently measured by hand). A stronger resonance should be obtained by increasing the precision of all components and better isolating the functional layer from the PDMS above and below. Information about the durability of the device is also needed.

SAW STRAIN SENSOR

Fabrication

Device Structure: The final evaluated device consisted of a base layer of thermal release tape (TRT), a layer of PMMA, a transferred gold IDT pattern, and a 300nm-thick layer of GaN. The project goal was to replicate the strain-sensing results from Kim et al. [6] – as the sensor experiences a bending condition, the resonant frequency of the device should shift in a predictable manner. This is observed due to the piezoelectric properties of GaN – when a signal is fed into the electrode pad, the IDT pattern supplies the electrical signal to the GaN membrane. The GaN membrane then converts the electrical signal into mechanical oscillations (surface acoustic waves), which in turn influence the electrical signal. As the GaN is bent in different ways, the resonant frequency is expected to shift, which can be detected using a vector network analyzer [6].

The IDT Electrode Pattern

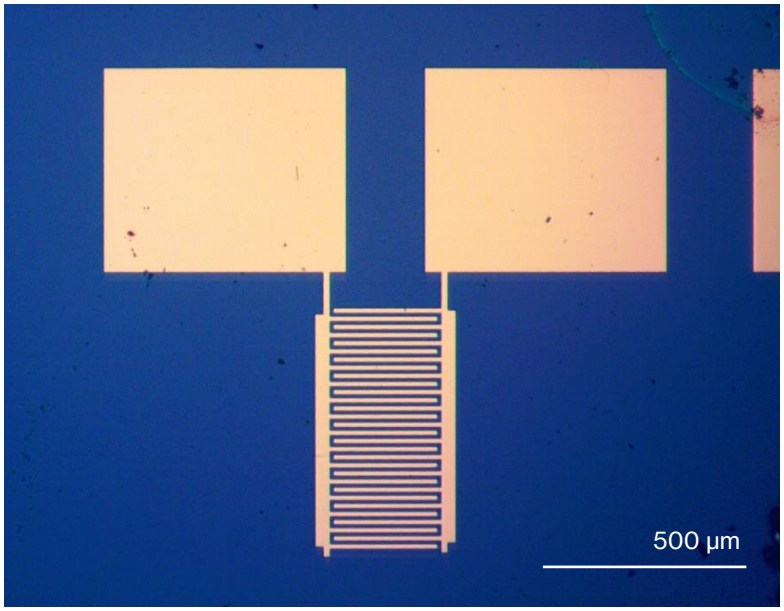

Figure 9 – Optical microscope image of the gold IDT electrode design. Each digit is 10 µm wide with a 10 µm gap, 270 µm long, and 40 nm thick.

The electrode patterns were prepared by Sanggeun Bae on Si-SiO_2 substrates using deposition and lithography techniques.

Figure 10 – Images of the IDT patterns on Si-SiO_2 wafers. To the naked eye, the individual digits are not discernible. However, the iridescent diffraction effect they cause is quite noticeable.

Rigid Substrate Test: the IDT electrode pattern was originally created on a Si-SiO_2 wafer. A preliminary rigid device was made to test the resonant frequency of the device on the rigid substrate. A small piece of GaN (2mm x 2mm) was transferred on top of the IDT pattern, the PPC handling layer was etched off, and the S_{11} return loss was measured with the NanoVNA sweeping from 50 kHz to 100MHz.

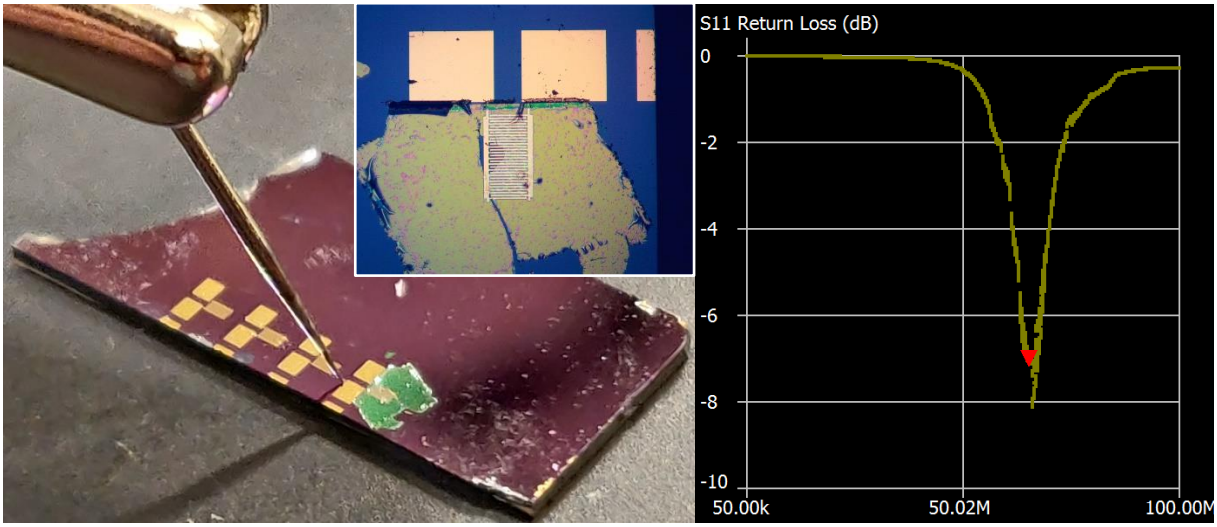

Figure 11 – Left: Preliminary device in testing setup. The needle probe is connected to the device via one electrode pad, and to the NanoVNA through the output port. Inset: Optical microscope image of the GaN transfer on top of the IDT pattern. Right: S_{11} graph showing a resonant frequency at ~70 MHz and ~-8 dB.

IDT Pattern Transfer to TRT + PMMA:

Si-SiO_2 wafers with IDT patterns were first cut into smaller pieces to create multiple separate samples. The wafers were cleaned with acetone and isopropyl alcohol and dried to prevent adhesion problems. Then, they were spin coated with PMMA at 800 rpm for 60 seconds, and cured on a hot plate at 120° C for 30 minutes. The thermal release tape was then adhered to the top surface of the PMMA, and the edges of the Si-SiO_2 wafer were scraped to ensure BOE could access the wafer in the next step – etching. The goal of the BOE etching was to remove the SiO_2 layer in order to separate the Au-PMMA-TRT from the Si below. This etching process took the better part of a day due to the substantial thickness of the SiO_2. After etching was complete, the TRT was then used to peel the device off of the Si wafer. This etching and liftoff step provided significant challenges and had a high failure rate – the fragile IDT patterns would often be damaged beyond usability while peeling off.

GaN Transfer: 2D GaN was sourced from a sample already detached from the original growth substrate. The source consisted of a TRT base, followed by Ni, Ti, and then GaN on top. To get the GaN as a freestanding membrane, the other layers needed to be removed. First, GaN samples were cut to size with scissors. They were then spin coated with PPC and cured at 90° C for 30 seconds. The edges of the sample were carefully trimmed to remove the PPC that had enveloped the sides of the sample. The hot plate was turned up to ~130° C and the samples were placed back on for another 10 minutes to detach the TRT. Once the Ni-Ti-GaN-PPC was free from the TRT, the samples were floated on the surface of a dish of DI water. The Ni layer was etched off in ferric chloride etchant solution, and the samples were rinsed thrice (refer to the TiO_2 transfer description from page 10). The Ti was etched in a similar process, except using buffered oxide etchant (BOE) containing hydrofluoric acid.

After this process, the samples remained only with the GaN and the PPC layer above it. These were carefully placed onto the IDT-patterned substrates using the same “fishing-out-of-water” technique used for MoS_2 and TiO_2 (refer to page 10). Because locational precision was extremely important for this device, it was helpful to use a squirt bottle of DI water to re-wet the surface of the substrate and allow the GaN membrane to be adjusted with tweezers, taking care not to damage or fold the membrane. Once the position was deemed satisfactory, a small scrap of a lab wipe was used to absorb the additional water and confirm the final position of the membrane (this technique was remarkably user-friendly and should be used whenever thin membrane transfer is needed). For the final device, the PPC on top of the GaN membrane was unable to be etched off,

because the PMMA substrate would be inadvertently damaged in the process. It was also planned to remove the TRT from the PMMA, but doing so would have damaged the device, as the PMMA was too fragile on its own.

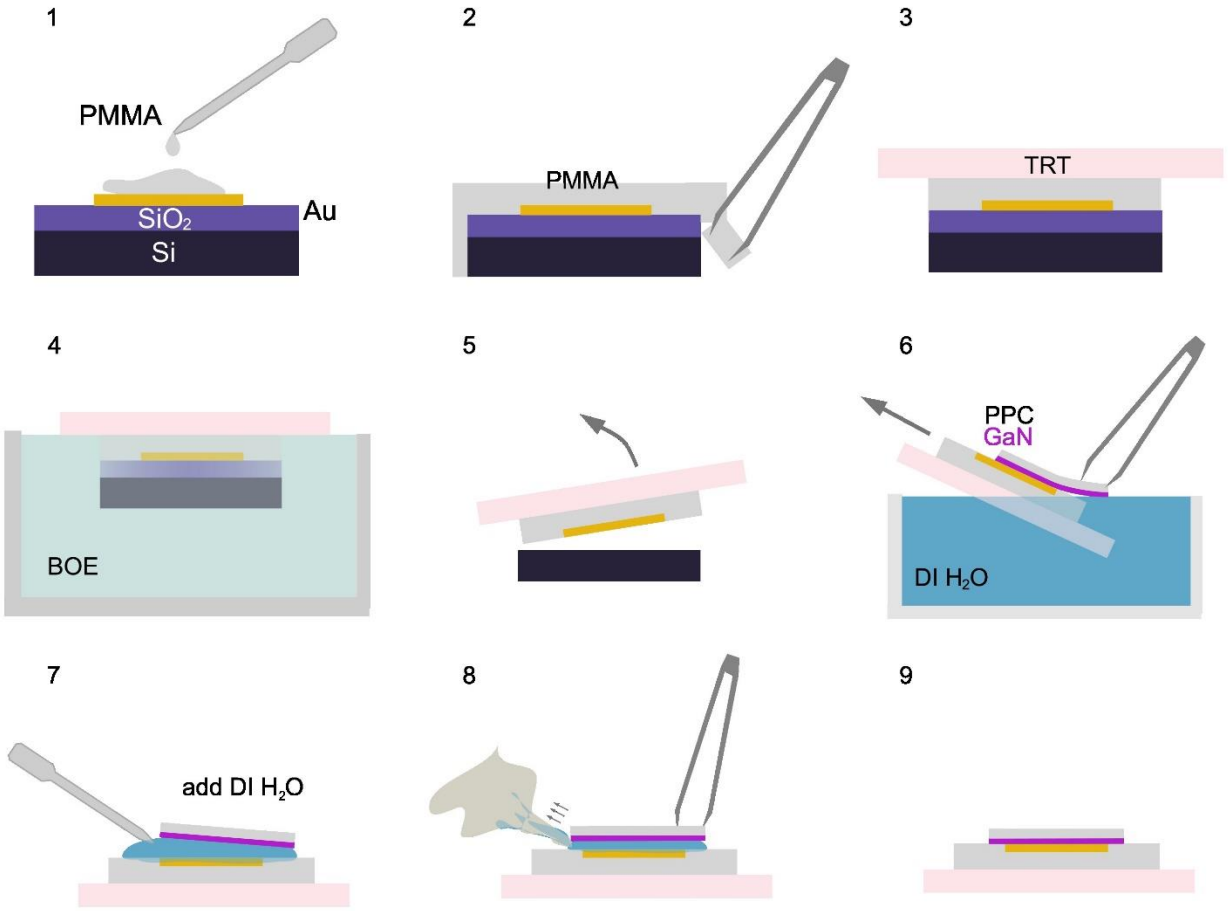

Figure 12 – Illustrated schematic process used in making the SAW strain sensor. 1) spin coat PMMA. 2) scrape excess PMMA off edges after curing. 3) add TRT. 4) etch away SiO_2 in BOE. 5) detach from wafer. 6) add GaN membrane. 7) add water to facilitate position adjustment. 8) adjust GaN placement and wick away water when satisfactory. 9) let dry – this is the final product we reached, however, the ideal device would not have TRT or the top layer of PPC.

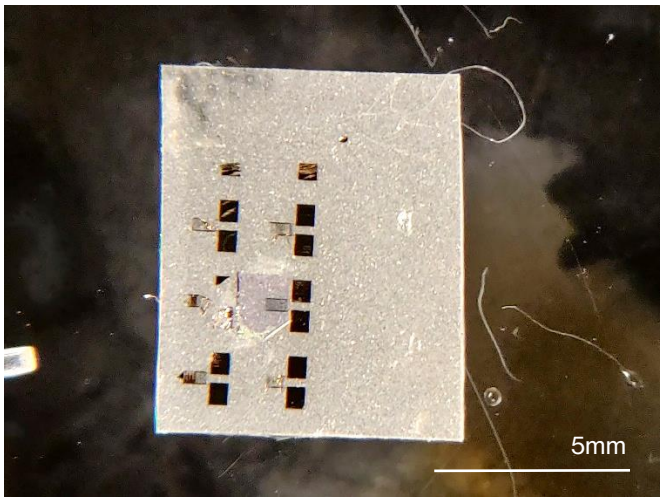

Figure 13 – Image taken of the final device through a magnifying glass. The gray translucent substrate is the TRT, and the PMMA above it is hardly visible. Of the six copies of the pattern on this sample, only one was in good enough condition for the GaN to be placed on top. The square with a slight purple tint is the GaN.

Analysis

To validate the basic phenomenon of resonant frequency shifting due to strain, the resonant frequency of the device was tested while flat, bent convex (tensile strain condition), and concave (compressive strain condition). For the bent conditions, the radius of curvature was approximately 1 cm. The measurements were done with the NanoVNA with one probe in contact with one of the electrode patches of the device. The input signal frequency was swept from 40 to 100 MHz. The resonant frequency was defined to be the frequency at which the minimum voltage standing wave ratio (VSWR) was achieved.

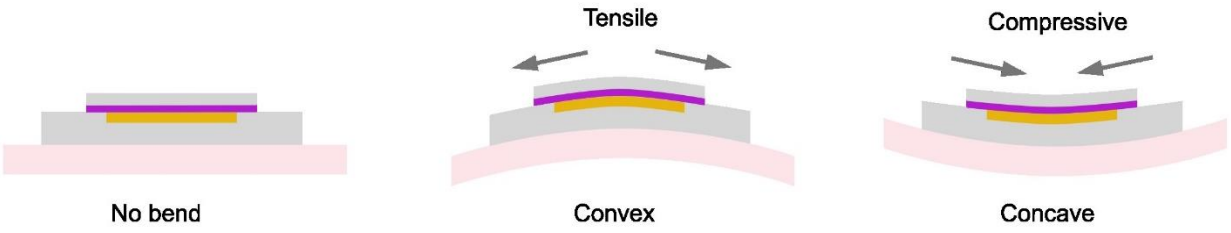

Figure 14 – Clarification of bend conditions.

The following data was extracted:

Convex: Min VSWR 5.854 @ 58.5390 MHz, Return Loss -2.997 dB

Not bent: Min VSWR 5.823 @ 58.3845 MHz, Return Loss -3.013 dB

Concave: Min VSWR 5.697 @ 58.087 MHz, Return Loss -3.081 dB

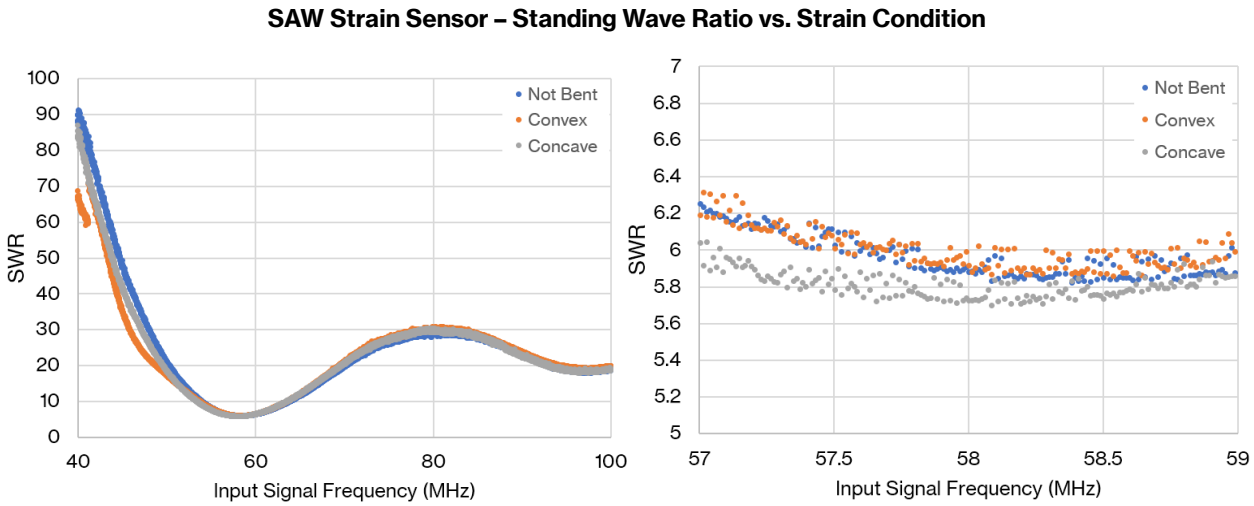

Figure 15 – Graphs of VSWR vs. input signal frequency for each strain condition. Left: Curves for the entire sweep range. Right: zoomed in graph of the resonant area of the curves. The shift in resonant frequency appears to be very slight but comparable to the shifts observed in Kim et al. [6]

The frequency shift observed in the three trials exhibit the same phenomenon observed in Kim et al [6]. However, the troughs where the resonant frequencies occurred were much more spread out, and the minimum VSWR is much higher than desired. It is likely that the GaN may have been damaged during the transfer process due to hand operation and was no longer perfectly monocrystalline. In addition, the strain sensor was unable to be removed from the TRT, which defeats its ability to be wearable – the TRT is much too thick and rigid. For a future attempt to improve this device, more sweeps should be done at different curvatures to confirm the relationship between strain and frequency shift.

ABBREVIATIONS

BOE – buffered oxide etchant

IDT – interdigitated

PDMS – polydimethylsiloxane (dimethicone)

PMMA – polymethyl methacrylate

PPC – polypropylene carbonate

SAW – surface acoustic wave

TRT – thermal release tape

VNA – vector network analyzer

VSWR – voltage standing wave ratio

REFERENCES

[1] Meng, Y., Feng, J., Han, S. *et al.* Photonic van der Waals integration from 2D materials to 3D nanomembranes. *Nat Rev Mater* **8**, 498–517 (2023). https://doi.org/10.1038/s41578-023-00558-w

[2] Pham, P.V., Bodepudi, S.C., Shehzad, K. *et al.* 2D Heterostructures for Ubiquitous Electronics and Optoelectronics: Principles, Opportunities, and Challenges. *Chemical Reviews* **122 (6)**, 6514-6613 (2022). DOI: 10.1021/acs.chemrev.1c00735

[3] Kum, H.S., Lee, H., Kim, S. *et al.* Heterogeneous integration of single-crystalline complex-oxide membranes. *Nature* **578**, 75–81 (2020). https://doi.org/10.1038/s41586-020-1939-z

[4] Hassanien, A.E., Breen, M., Li, MH. *et al.* Acoustically driven electromagnetic radiating elements. *Sci Rep* **10**, 17006 (2020). https://doi.org/10.1038/s41598-020-73973-6

[5] Joy, B., Cai, Y., Bono, D.C. *et al.* Cell Rover – a miniaturized magnetostrictive antenna for wireless operation inside living cells. *Nat Commun* **13**, 5210 (2022). https://doi.org/10.1038/s41467-022-32862-4

[6] Kim, Y., Suh, J.M., Shin, J. *et al.* Chip-less wireless electronic skins by remote epitaxial freestanding compound semiconductors. *Science* **377**, 859-864 (2022). DOI: 10.1126/science.abn7325